Applications of Active Arrayed-Waveguide Gratings in Dynamic WDM Networking and Routing

Michael C. Parker, *Associate Member, IEEE, Member, OSA*, Stuart D. Walker, Augustin Yiptong, and Robert J. Mears

***Abstract*—We describe how active arrayed-waveguide gratings (AWGs) may find a diverse range of applications in future dynamic wavelength division multiplexed (WDM) networking and routing. Our initial simulations indicate that these applications include dynamic signal power and erbium-doped fiber amplifier (EDFA) gain equalization with a dynamic range of 12 dB, and interchannel amplified spontaneous emission (ASE) suppression by more than 20 dB; optical add/drop multiplexing with passband-flattened channels and suppressions of 15 dB; and dynamic dispersion compensation of up to ±300 ps/nm.**

***Index Terms*—Fourier transforms, gratings, integrated optics, optical equalizers, optical planar waveguide components, photonic switching systems, waveguide arrays, wavelength division multiplexing.**

I. Introduction

As a result of intense international effort, the requirements for future erbium-doped fiber amplifier (EDFA)-based wavelength-routed networks are now becoming more clearly defined [1]. In addition to existing gain equalization features, a need for dynamically reconfigurable add/drop multiplexing, space/wavelength switching and dispersion compensation is emerging [2], while time synchronization in IP-routed networks is also becoming an issue. The arrayed-waveguide grating (AWG) [3], [4] is an increasingly important wavelength division multiplexed (WDM) technology for passive (de)multiplexing and fixed wavelength routing [5], [6]. In previous work [7], [8], we have shown how active AWGs can provide some aspects of WDM networking functionality by phase and/or amplitude wavefront profiling. However, the delivery of all these features in an active AWG has not, to our knowledge, previously been discussed. In this paper, we describe how dynamic phase-profiling can provide all these desirable properties. In particular, we report simulation results which show how holographic techniques [9] based on the simulated annealing algorithm can offer good agreement with target functions obtained by either analytical or experimental means. Attractive features of active AWG devices potentially include: multi-wavelength control, nonmechanical operation and compact realization.

Manuscript received April 4, 2000; revised September 15, 2000.

M. C. Parker is with Fujitsu Telecom Europe Ltd. Research, Colchester, Essex CO3 4HG, U.K. (e-mail: M.Parker@ftel.co.uk).

S. D. Walker is with the Department of Electronic Systems Engineering, University of Essex, Colchester, Essex CO4 3SQ, U.K. (e-mail: stuwal@essex.ac.uk).

A. Yiptong and R. J. Mears are with the Department of Engineering, University of Cambridge, Cambridge CB2 1PZ, U.K. (e-mail: rjm@eng.cam.ac.uk).

Publisher Item Identifier S 0733-8724(00)10700-5.

II. Fresnel–Kirchhoff Diffraction Theory Applied to AWGs

Fourier optics provides an excellent framework for understanding the operation of the AWG [10]–[12], enabling the free-propagation regions to be modeled using first-order diffraction theory. The Fresnel–Kirchhoff diffraction integral for the free-space propagation of light through an aperture S in the ε–η plane after a distance s' is given by [13]

$$U(x, y) = -j\frac{\cos\delta}{\lambda}\frac{Ae^{jkr'}e^{jks'}}{r's'}\iint_S e^{jkf(\varepsilon,\eta)}\,d\varepsilon\,d\eta \quad (1)$$

where U is the far-field distribution of light in the x–y plane. In the conventional derivation above, the aperture S is assumed to be illuminated by a spherical wavefront arriving at the screen, having propagated from a point source a distance r' behind the screen. The illumination function of the aperture is therefore given by

$$A(\varepsilon, \eta) = \frac{Ae^{jkr'}}{r'} \quad (2)$$

where the wavenumber of the incident light is given by $k = 2\pi/\lambda$. However, in our analysis, we are not concerned with a point-source origin of the light illuminating the aperture. Rather, we assume a general illumination function $A(\varepsilon, \eta)$ of the aperture, to yield a modified Fresnel–Kirchhoff diffraction integral formula

$$U(x, y) = -j\frac{\cos\delta}{\lambda}\frac{e^{jks'}}{s'}\iint_S A(\varepsilon, \eta)e^{jkf(\varepsilon,\eta)}\,d\varepsilon\,d\eta \quad (3)$$

where

$$f(\varepsilon, \eta) = -\frac{x\varepsilon + y\eta}{s'} + \frac{\varepsilon^2 + \eta^2}{2s'} - \frac{(x\varepsilon + y\eta)^2}{2s'^3} + \cdots \quad (4)$$

For the AWG geometries in which we are interested, especially that of the free propagation region (FPR), as shown in Fig. 1, the array of waveguides are arranged on a Rowland circle configuration, so that the high orders in the function $f(\varepsilon, \eta)$ die away rapidly. The factor $\cos\delta$ is the angle between the optical axis of the system and the aperture plane, and is close to unity. As is well known, when the quadratic and higher orders of ε and η [as given in (4)] can be neglected, (3) collapses to a Fourier transform (FT) integral, and Fraunhofer diffraction takes place. When the quadratic terms cannot be neglected, we have instead Fresnel diffraction taking place. Both truncations of the function can be considered to be paraxial approximations to the optical

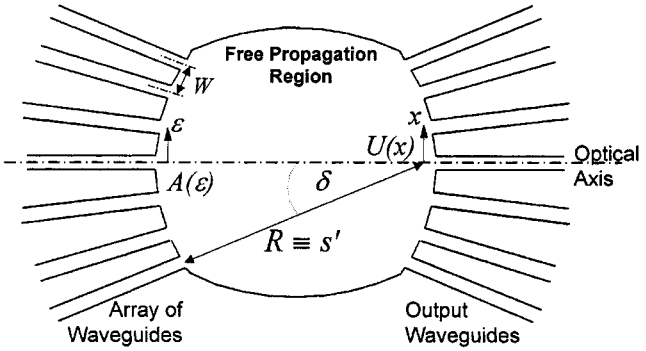

Fig. 1. Application of Fresnel–Kirchhoff diffraction integral to the planar free-propagation region in an AWG.

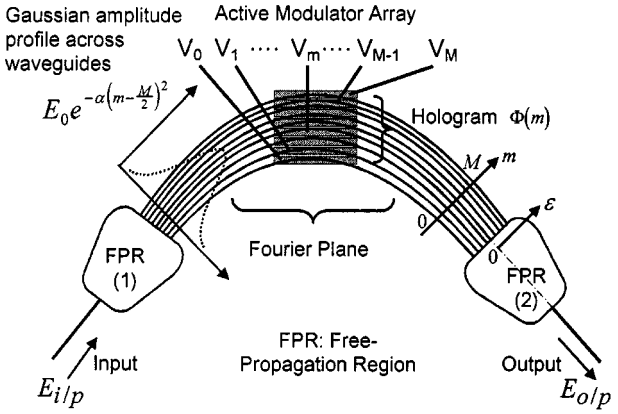

Fig. 2. Schematic of active holographic AWG, with phase-modulators in the Fourier plane.

system, and are analyzed in this paper as they find useful applications, and yield physical insight into the processes involved. As AWGs have an essentially planar geometry, with free-propagation within the plane of the device, diffraction only occurs in two dimensions so that the Fresnel–Kirchhoff integral reduces to a one-dimensional (1-D) formula, with only ε and x being the complementary space variables. Each side of the free propagation region is adjoined by an array of waveguides, which effectively cause the aperture to be discretised into multiple apertures. This can then be mathematically modeled by replacing the continuous integral of the Fresnel–Kirchhoff formula with a discrete series summation.

III. Fourier Holographic Techniques for AWG Passband Control

A. Optical Fourier Transform Theory

The two FPRs on either side of the arrayed-waveguide section (equivalent to the Fourier plane [11]) of an AWG allow the overall device to be considered as a planar $4f$ lens-relay system. Hence, the techniques of spatial filtering associated with free-space versions of such systems can also be applied to AWGs. Holographic techniques, based on FT theory, are emerging as a powerful tool to tailor the spectral-response of grating-based [9], [14] WDM optical devices, and achieve multi-wavelength control. Arbitrary segmented passbands with variable transmissions are possible, as well as apodization and passband shaping to yield near-rectangular filter responses [15]. Since the basic Fraunhofer diffraction integral of (3) is essentially an FT, holographic techniques can therefore also be applied to AWGs. Holographic filtering based on phase-only conditioning of the Fourier-plane of the AWG is attractive since it implies optimum use of the available light, due to avoidance of unnecessary attenuation. However, full complex (amplitude and phase) control can also be employed by selective attenuation or gain within individual waveguides (in addition to phase-control) so as to achieve a continuous complex Fourier function. Fig. 2 shows a holographic AWG, with phase-only spatial filtering at the Fourier plane by means of an array of phase-modulators, which constitutes the hologram. Such a device has already been demonstrated [16], with the phase modulators acting to correct for phase errors occurring during fabrication. When the quadratic terms of $f(\varepsilon, \eta)$, as indicated in (4), are excluded from the integral of (3), we can write the 1-D version of the Fresnel–Kirchhoff formula in its FT representation, so that the AWG output electric field $E_{o/p}(x)$, or FT of the aperture function $A(\varepsilon)$ is given by

$$E_{o/p}(x) = \frac{-j}{\sqrt{\lambda R}} \int_{-\infty}^{\infty} A(\varepsilon) e^{-j(2\pi n/\lambda R)x\varepsilon}\, d\varepsilon \tag{5}$$

where R is the length of the FPR, n is the refractive index, and $A(\varepsilon)$ is the product of the phase hologram $\Phi(\varepsilon)$ transfer function across the arrayed-waveguides, and an overall Gaussian amplitude distribution, such that

$$A(\varepsilon) = E_0 e^{-\alpha(\varepsilon^2/W^2)} e^{j\Phi(\varepsilon)} \tag{6}$$

with α defining the width of the Gaussian function.

However, for a fixed spatial position x of the output waveguide, the integral (5) can also be considered as variable in wavelength λ, meaning that the equation can also be considered as a filter spectral transmission equation $E_{o/p}(\lambda)$. By employing a discrete Fourier series formalism, (5) can therefore be expressed as the following series summation:

$$E_{o/p}(\lambda) = \frac{-jWE_0}{\sqrt{\lambda R}} \sum_{m=0}^{M} \cdot e^{-\alpha(m-(M/2))^2 + j(2\pi n \Delta l/\lambda)m + j\Phi(m)} \tag{7}$$

where W is the arrayed-waveguide spacing (see Fig. 1), Δl is the incremental pathlength difference between neighboring waveguides, and there are $M+1$ waveguides in the array. The electric field E_0 at the center waveguide of the array is related to the input electric field, $E_{i/p}$, by $E_0 \approx -ja\sqrt{(\pi/\lambda R)}E_{i/p}$, where a is the spot size of the mode in the input waveguide to FPR(1). A more accurate mathematical model would convolve the implicit delta-function representation of each waveguide with the guided-mode structure of the light within the waveguide. However, the guided-mode (an approximate Gaussian intensity distribution) merely changes the overall envelope of the far-field intensity distribution, and can be neglected in the analysis. The phase hologram $\Phi(m)$ normally has a small wavelength sensitivity depending on its implementation. This would be the case, for example, if one varied the optical pathlengths of the individual waveguides. Phase control of each

arm can be achieved by actively altering the local refractive index [17] of the individual waveguides. The phase changes (ranging from $-\pi$ to $+\pi$) required in each waveguide arm need only be imposed over a short length of the arm, depending on the strength of the electro-optic or thermo-optic effect used to introduce the phase change. The desired phase change ϑ_m for the mth arm will only be correct for a particular wavelength, e.g., $\lambda_0 = 1550$ nm. A wavelength at the edge of the Erbium window, say $\lambda_1 = 1530$ nm, would experience a phase change of $\vartheta_m \times \lambda_1/\lambda_0$, i.e., it would be out by 20 parts in 1550 or only about 1.3%; but this is independent of the number of grating arms, and the size of the hologram. The hologram can be considered to be an additional first-order grating superposed onto the conventional (high order $\sim$50) AWG grating, respectively, with the first-order grating having less wavelength dependence.

B. Design of Holograms

Since the functionality of the holographic AWG is ultimately expressed by the FT of the aperture function $A(\varepsilon)$, the phase hologram $\Phi(\varepsilon)$ is designed by tailoring its spatial distribution across the arrayed-waveguides so that its spectral response (i.e., the FT of its spatial distribution) has the form of the desired filtering function. Superficially, the required spatial distribution is just the inverse FT of the desired spectral response. However, the inverse FT of a desired spectral distribution function will tend to yield a complex spatial distribution. This is equivalent to a spatial distribution containing both dielectric and absorptive components. However, we are generally only interested in a filtering function with a certain amplitude response (e.g., for power equalization, add/drop multiplexing, etc.). This implies that just the modulus (or the amplitude) of the spectral distribution is of interest, while its phase characteristic can be neglected. If we allow the phase characteristic to be a degree of freedom, we can design a hologram consisting of only a real refractive index distribution across the waveguide arms. The FT of that spatial distribution will yield a spectral distribution with the desired amplitude distribution, but with an arbitrary phase characteristic. A suitable spatial distribution thus has to be calculated which is purely real, yet whose FT yields the desired spectral amplitude response. Constraints are placed on this calculation in each of the complementary FT planes ε and x (or equivalently λ), respectively. The first is that the hologram $\Phi(\varepsilon)$ must be purely real, while the second is the actual amplitude characteristic of the target spectral distribution (i.e., filtering function). Together, these two constraints make the calculation of the hologram a nondeterministic problem, best solved using optimization algorithms such as simulated annealing [18] (as used to generate the holograms simulated in this paper), error-diffusion [19] or genetic algorithms, etc. Fig. 3 shows (in 4-bit gray-scale) two generated phase-holograms, designed for spectral power equalization and optical add/drop multiplexing functionalities, respectively.

For functionalities such as multi-wavelength dispersion compensation, where the phase characteristic of the spectral distribution is important (i.e., dispersion characteristic is given by the second differential of the phase characteristic), a further constraint must be introduced into the calculation. Instead of just requiring a certain magnitude for the spectral distribution response, we must consider both the real and imaginary amplitude characteristics.

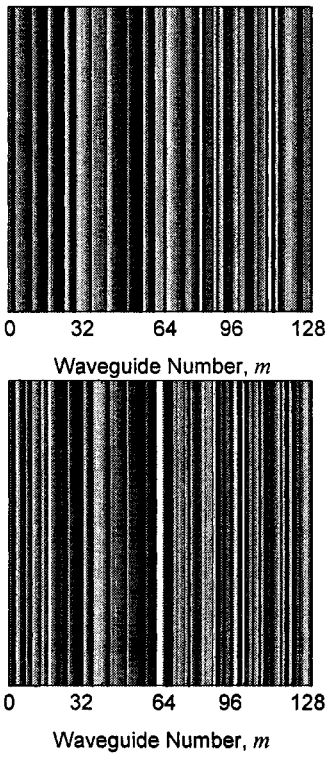

Fig. 3. Example 4-bit phase-holograms, generated using the simulated annealing optimization algorithm. Gray-scale, 4-bit (16 levels) representation of phase: black$=0$, white$=2\pi$.

C. Power and EDFA Gain Equalization

As the number of WDM channels is increased, the demand for well-specified spectral equalization of optical amplifiers becomes more urgent. If, as seems likely, there is a move toward greater optical transparency in switching, the need for dynamic control of WDM channels will become paramount. AWG devices using a similar arrayed-waveguide phase-modulation technology have already been demonstrated [20], but the active waveguide array has been positioned within a Mach–Zehnder configuration rather than in the Fourier-plane of the AWG. In the case of individual phase-modulator failure, the Fourier-plane configuration will integrate the loss in performance across the spectral range of operation, whereas the Mach–Zehnder embodiment will tend to suffer the complete loss of a channel. The holographic designs presented here are realized by allowing the deviation in the optical pathlength of successive waveguides to differ from their usual relationship by up to $\pm\pi$, with a quantization of four bits. Four bit hologram quantization allows the errors between the target filtering function and the AWG response to be reduced to less than 1 dB. In our simulation, we have designed a dynamic spectral equalizer [21] to compensate for a (hypothetical) 12 dB dynamic range over the EDFA amplifier passband. Fig. 4(a) depicts the simulated transmission results for an AWG consisting of 128 active arrayed-waveguides, with a free-spectral range (FSR) equal to 6.4 nm, equalizing 8×100 GHz channels over a 12 dB dynamic range. We have assumed a uniform illumination of

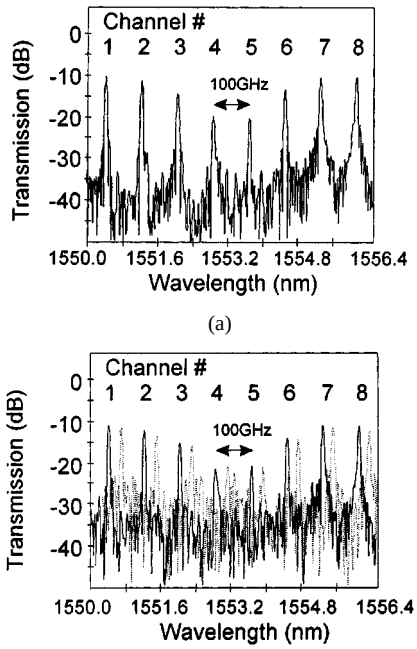

Fig. 4. (a) Simulation results for active holographic AWG functioning as an equalizing (12 dB) filter. (b) Effect of random pathlength jitter of $\lambda/8$ and $\lambda/4$ (dashed and offset).

the Fourier plane, such that the Gaussian intensity parameter $\alpha = 0$. In addition to the equalizing functionality, good interchannel amplified spontaneous emission (ASE) suppression of greater than 20 dB is also achieved. Note that the cyclical frequency response of the AWG would allow this technique to be simply extended, for example to the control of 80 channels, by preceding ten of these active AWGs by a passive passband-flattened (3-dB width = 6.4 nm) conventional AWG of FSR=64 nm.

Of great importance is the robustness of this design to fabrication tolerances. In order to test this, varying levels of random pathlength "jitter," corresponding to $\lambda/16$; $\lambda/8$; $\lambda/4$ and $\lambda/2$ of the total optical pathlength deviation in the design have been simulated. The results are encouraging—the effect is barely noticeable at the $\lambda/16$ level and at $\lambda/8$ there is a small additional excess loss ($\sim$1 dB) with little distortion of the passband shape. The design begins to break down for a pathlength jitter of $\lambda/4$, as shown in Fig. 4(b), where the noise floor rises appreciably to give crosstalk of greater than -10 dB.

D. Optical Add/Drop Multiplexing

The very good interchannel suppression suggests that the filter design algorithm can also be used to realize arbitrary channel dropping (/combining) filters. As an example, we present the same active AWG filter, but with a filter response designed to pass channels 1, 2, 4, 6, 7, 8 and drop (suppress) channels 3 and 5. Fig. 5 shows the simulated filter response. The filter design algorithm has also been adapted to enable near-rectangular passband flattening, as is evident in the figure, so demonstrating the flexibility of the holographic technique. This makes the device more robust to laser wavelength fluctuations, as well as temperature effects. However, this is at the

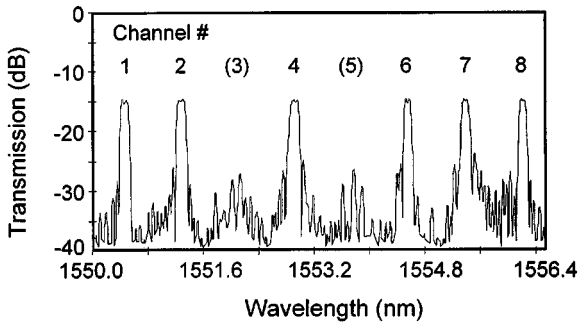

Fig. 5. Simulation results for an active holographic AWG designed as a channel dropping filter, demonstrating OADM functionality.

expense of channel suppression of only 15 dB, and a greater device insertion loss. A higher number of arrayed-waveguides, and/or a reduced degree of passband broadening would improve both these figures.

E. Holographic AWG Excess Insertion Loss

An active InP-substrate AWG with individual phase control for 48 arms of the arrayed-waveguide section has been fabricated to exhibit an insertion loss of 3 dB [16]. Phase control of the device's Fourier plane was used to achieve closer performance to the theoretical sinc response of a uniform grating structure. However, the implementation of a hologram in the Fourier plane via phase control, disrupts the uniform grating structure. This results in an overall insertion loss increase, as the grating becomes less efficient at directing light to the output port. In general, the excess insertion loss increases with the number of channels being controlled C as $10\log_{10} C$, or $10\log_{10} 3C$ for flattened passbands [22]. For example, Fig. 4 depicts the transmission spectrum for a holographic AWG equalizing $C = 8$ channels. Hence, the insertion loss for the channel experiencing least attenuation would be expected to be of the order $10\log_{10} 8 = 9$ dB, as indicated by the figure. Likewise, Fig. 5 shows the spectral response for an active AWG with OADM functionality, controlling $C = 6$ passband-flattened channels. In this case, the excess insertion loss is expected to be close to $10\log_{10}(3 \times 6) = 12.6$ dB, again as indicated in the figure. Although this loss is relatively large for the small channel count C considered here, for larger C it increases only marginally (i.e., logarithmically), and so scales well for a large WDM channel count.

IV. Dynamic Dispersion Compensation

As channel bit-rates in optical networks increase, physical layer temporal dispersion in dense WDM networks is becoming an important consideration. Dispersion compensation (DC) techniques are now seen as a critical element in the design of future high-capacity lightwave communication systems. Passive DC using fiber Bragg gratings is well established [23] with dynamic DC also recently being demonstrated [24]. Fixed DC using a passive chirped AWG has been suggested [25], [26], but we now propose how dynamic DC can be achieved with an active AWG. The variable time delay associated with dynamic DC means that such an AWG may also find application as a

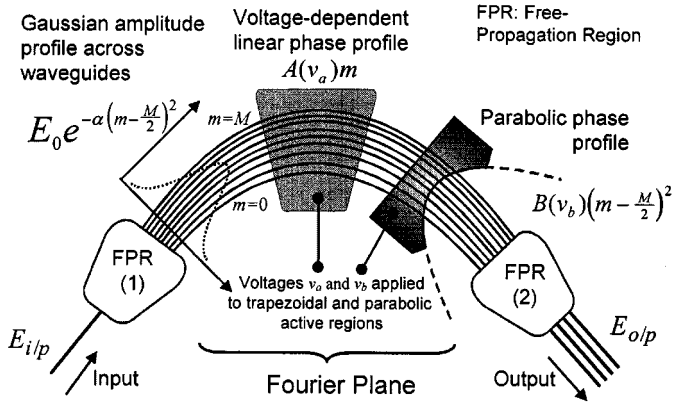

Fig. 6. Schematic of dynamic dispersion compensating AWG, using parabolic and trapezoidal active regions in the Fourier plane.

multi-wavelength, tunable delay line in IP-routed packet-based optical networks.

A. Hybrid Fourier-Fresnel Diffraction

Fig. 6 shows a schematic of an active AWG with an active symmetric parabolic phase profile and an active trapezoid imposed on its central arrayed-waveguide region. The trapezoidal region can be used to allow the active AWG to function as a space-wavelength switch [6], while the parabolic phase profile effectively chirps the AWG grating, and allows dispersion compensation. With reference to Fig. 6, the following discrete summation describes the output electric field from the AWG

$$E_{o/p}(\lambda) = \frac{-jWE_0}{\sqrt{\lambda R}} \sum_{m=0}^{M} \cdot \exp\left(j\frac{2\pi n\Delta l}{\lambda}\left[1+A(v_a)-\frac{xW}{R\Delta l}\right]m + \left(j\frac{2\pi n\Delta l B(v_b)}{\lambda}-\alpha\right)\left(m-\frac{M}{2}\right)^2\right) \quad (8)$$

where $B(v_b)$ is the strength of the induced parabolic phase shift, equivalent also to the degree of chirp imposed on the device. Apparent are the functional similarities between (8) and (3), and (4), as they both have linear and quadratic terms, so indicating that hybrid Fourier–Fresnel diffraction is taking place. By approximating the series summation (8) to a continuous integral-based formalism, the transmission transfer function can be written as a series of Fresnel integrals

$$t(\lambda) = \frac{E_{o/p}}{E_{i/p}} \approx -\frac{aW}{\lambda R}\frac{\pi}{\sqrt{2}}\frac{M}{2b}\left\{C_1(a+b)-C_1(a-b) + jS_1(a+b)-jS_1(a-b)\right\}e^{j\phi} \quad (9)$$

where C_1 and S_1 are the Fresnel cosine and sine integrals of the first kind [27]. The normalized parameters a, b, and ϕ are given as follows:

$$a = \frac{\pi(\lambda_0-\lambda)}{2\text{FSR}\sqrt{\frac{\pi\lambda_0 B(v_b)}{2\text{FSR}}+j\frac{\alpha}{4}}} \quad (10a)$$

$$b = M\sqrt{\frac{\pi\lambda_0 B(v_b)}{2\text{FSR}}+j\frac{\alpha}{4}} \quad (10b)$$

$$\phi = \frac{M\pi(\lambda_0-\lambda)}{\text{FSR}} - \frac{\pi^2(\lambda_0-\lambda)^2}{4\text{FSR}^2\left(\frac{\pi\lambda_0 B(v_b)}{2\text{FSR}}+j\frac{\alpha}{4}\right)} \quad (10c)$$

with λ_0 being the central wavelength of the passband, and FSR $= \lambda^2/n\Delta l$ the device free-spectral range (FSR). As might be expected, this describes the typical passband response of a linearly-chirped grating structure [28]. The linear coefficient term $[1+A(v_a)-(xW/R\Delta l)]$ does not appear explicitly in (9) and (10) as it only determines the central wavelength λ_0 of the AWG passband given by

$$\lambda_0 = \sqrt{\text{FSR}n\Delta l}\left[1+A(v_a)-\frac{xW}{R\Delta l}\right]. \quad (11)$$

It is apparent from (11) that the central wavelength λ_0 can be tuned both by applying a voltage v_a to the trapezoidal electrode to vary the coefficient $A(v_a)$, forming the basis of a space-wavelength switch; and by the spatial position x of the output waveguide, i.e., the demultiplexing functionality of a conventional passive AWG. It should be noted that terms associated with the parabolic phase profile, such as the voltage-dependent coefficient $B(v_b)$ do not appear in (11). This is because a symmetric parabolic phase profile does not detune the AWG. Instead, the voltage-dependent coefficient B (where the v_b dependence is implicit) acts only to independently control the degree of dispersion compensation. The total AWG phase response $\theta(\lambda)$ is a combination of three factors: linear and broadly parabolic terms about λ_0, corresponding to the phase profile $\phi(\lambda)$ of (10c); and an additional phase response due to the Fresnel integrals, which follows the form of the Cornu spiral [29]. Dispersion characteristic is defined as the second frequency derivative of the AWG phase response $\theta(f)$ [25], but can be closely approximated in the following manner:

$$D = \frac{\partial\tau_d}{\partial\lambda} \approx \frac{\lambda_0^2}{2\pi c}\frac{\partial^2\theta(\lambda)}{\partial\lambda^2} \quad (12)$$

where c is the speed of light. Using (9), the dispersion characteristic at the passband center wavelength λ_0 is thus analytically given by

$$D = \frac{1}{c}\left(\frac{M\lambda_0}{2\text{FSR}}\right)^2 \cdot \text{Re}\left\{\frac{\pi}{b^2}-\frac{\sqrt{2\pi}}{b}\left(\frac{C_1[b]\cos b^2+S_1[b]\sin b^2}{C_1^2[b]+S_1^2[b]}\right)\right\}. \quad (13)$$

For small degrees of chirp, the dispersion increases linearly with the voltage-dependent coefficient B, and is approximately given by

$$D \approx \frac{1}{c}\left(\frac{M\lambda_0}{2\text{FSR}}\right)^2\frac{2\pi}{45}\left[1-\frac{12\alpha^2}{315}-O\left(\alpha^4\right)\right]F \quad (14)$$

where we have introduced the normalized chirp parameter F, which while being proportional to B, is essentially independent

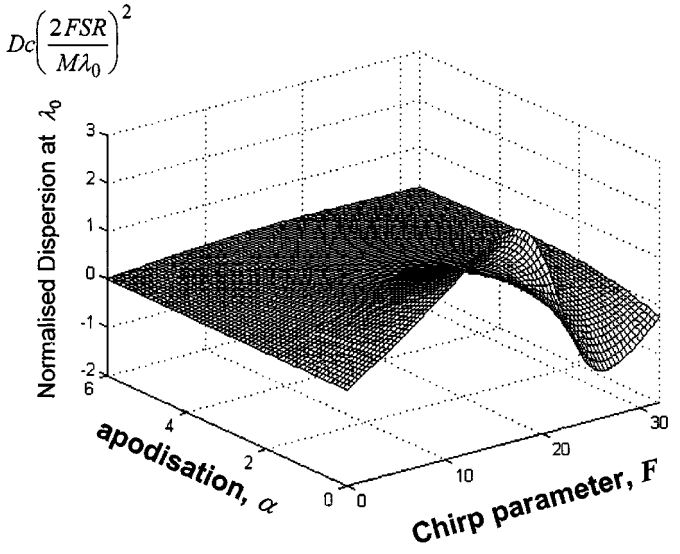

Fig. 7. Mesh plot of variation of normalized dispersion, with chirp parameter F, and Gaussian apodization parameter α.

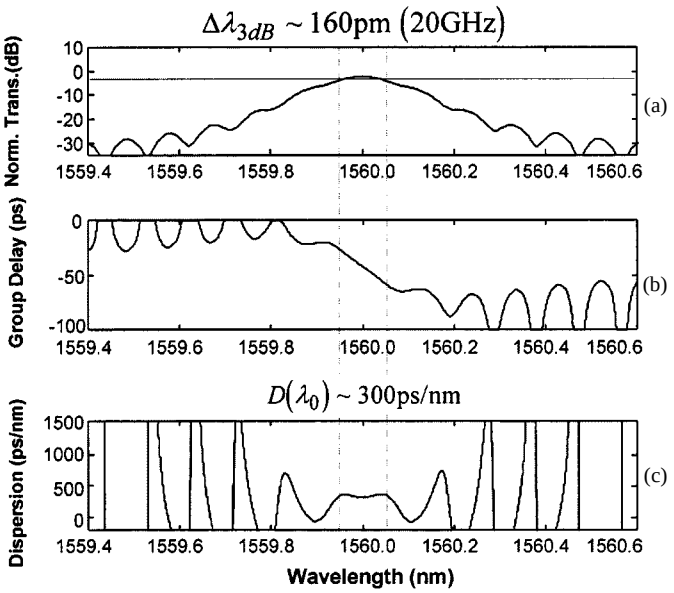

Fig. 8. Typical spectral plot $|t(\lambda)|^2$, group delay τ_d, dispersion characteristic $D(\lambda)$.

of the AWG parameters such as FSR, number of arrayed-waveguides M, and wavelength of operation λ_0

$$F = \frac{2\pi M^2 \lambda_0}{\text{FSR}} B. \tag{15}$$

Fig. 7 shows a three-dimensional mesh plot of the variation of normalized dispersion $D \cdot c(2\text{FSR}/M\lambda_0)^2$ as it varies with chirp parameter F, and Gaussian apodization parameter α. Apparent is the initial linear increase in dispersion with chirp F, in accordance with (14), until a maximum is reached for $F = 17.6$, when $D \cdot c(2\text{FSR}/M\lambda_0^2 = 2.5$. The degree of dispersion then rapidly reduces, and oscillates with reduced amplitude about zero in agreement with (13). The dispersion ripple across the 3-dB passband width also becomes increasingly evident with large chirp parameter F, so that chirping with $F > 17.6$ is not likely to yield a useful device. Fig. 7 and (14) also indicate that dispersion is maximized when the Gaussian parameter $\alpha = 0$, i.e., for a uniform power distribution along the arrayed-waveguides. However, the degree of ripple of the dispersion $D(\lambda)$ across the 3-dB passband width (i.e., the dispersion variance σ^2) is damped by α, and minimized for $\alpha \approx 4.5$, (see [30]), but at the expense of greatly reduced dispersion. In addition, the 3-dB AWG passband width $\Delta\lambda_{3\,\text{dB}}$ linearly increases with the chirp parameter F; the relationship [8] explicitly given by

$$\Delta\lambda_{3\,\text{dB}} \approx \Delta\lambda_0 + \frac{\pi \text{FSR}\lambda_0}{2\Delta\lambda_0} B = \Delta\lambda_0 \left(1 + \frac{F}{4}\right) \tag{16}$$

where $\Delta\lambda_0 = \text{FSR}/M$ is the 3-dB width of the unchirped, i.e., standard AWG. Apparent from (14) and (16) is that there is a maximum value of degree of dispersion compensation and 3-dB passband width available. Substituting the square of (16) into (14), and evaluating at $F = 17.6$, we find

$$D(\lambda_0) \cdot (\Delta\lambda_{3\,\text{dB}})^2 \leq 18\frac{\lambda_0^2}{c}. \tag{17}$$

Thus, for minimum dispersion ripple in the AWG passband, there is a fundamental limit to the passband width and degree of dispersion, set by the wavelength of operation λ_0 and the speed of light c.

B. Simulation Results

We have modeled an active AWG with FSR=12 nm ($\equiv 15 \times 100$ GHz), $\lambda_0 = 1560$ nm, refractive index $n = 2.2$, and 128 arrayed-waveguides, with chirp parameter $F = 11.2$, and Gaussian parameter $\alpha = 0.8$. Using the phase terms of (8), the required phase change ϑ_m as a function of B for the mth waveguide is given by

$$\vartheta_m = \frac{2\pi n \Delta l B}{\lambda} \left(m - \frac{M}{2}\right)^2. \tag{18}$$

For the longest waveguide, where $m = M$, the phase change is given by $\vartheta_M = 2\pi(n\Delta l M^2 B/4\lambda)$, where this phase change is accumulated only along an active section L_A, which is a proportion γ of the total waveguide length $L_M = M\Delta l$, so that $L_A = \gamma L_M$. The phase change ϑ_M is caused by an applied electric field altering the refractive index of the waveguide, where $\vartheta_M = 2\pi(L_A/\lambda)\Delta n$, with Δn being the change in refractive index. Equating the two expressions for the required phase change ϑ_M gives a relative refractive index change of $(\Delta n/n) = (BM/4\gamma)$, such that for dispersion compensation with $B = 8.37 \times 10^{-7}$, $\gamma = 0.4$, $M = 128$ waveguides, then $(\Delta n/n) = 66.9 \times 10^{-6}$. If the device is fabricated using Lithium Niobate, with linear electro-optic coefficient $r_{33} = 30.8 \times 10^{-12}\text{Vm}^{-1}$, and with refractive index change given by $\Delta n = (1/2)n^3 r_{33} E$, then the required electric field E applied to the waveguide is 900 kV/m. This is a modest applied electric field, requiring a voltage of 9.0 V for a waveguide thickness of 10 μm, over a maximum active length of $L_A = 4.8$ mm. Fig. 8(a) shows the normalized filter transmission response $|t(\lambda)|^2$, with the associated group delay τ_d, across the passband 3-dB width, shown in Fig. 8(b). The dispersion characteristic $D(\lambda)$ is plotted in Fig. 8(c), and is equal to ± 300 ps/nm across the 3-dB width of the filter passband, for

parabolic coefficient $B \sim \pm 8.37 \times 10^{-7}$. This would compensate 19 km of single-mode fiber (SMF) with a 16 ps/nm/km dispersion characteristic. With the Gaussian parameter optimized to $\alpha = 0.8$, slight variation in the dispersion characteristic of ± 7 ps/nm across the filter 3-dB passband width is still present. By designing the AWG to have a FSR of 15×100 GHz, the periodic nature of the spectral response can be taken advantage of to compensate for multiple channels, spaced by 12 nm on the ITU grid. The intermediate channels can be dispersion compensated by appropriate positioning of an additional 14 ports at the output of the device. An additional re-multiplexing AWG is required to multiplex all channels back onto a single fiber, to achieve in-line filtering.

By employing the device as a fine-tuning DC element, in conjunction with a fixed DC device (e.g., DC fiber) itself compensating for a fixed length of 80 km of SMF, the resulting adaptive DC unit can be used to compensate all 100 GHz DWDM channels for between 61 and 99 km of SMF. Such a device can be usefully employed in long-haul submarine or terrestrial systems, where automatic dispersion correction is a desirable feature. The variable dispersion feature may also be useful in all-optical IP routers where packet time alignment and jitter reduction are important issues.

C. Excess Insertion Loss due to Chirping of Waveguide Grating

Fig. 8(a) shows the normalized transmission of a chirped AWG. The chirping process is analogous to the effect of a defocusing lens causing a reduction in intensity of light at the focal plane, and will therefore introduce extra loss. Fig. 9(a) plots the relative excess insertion loss (in decibels) as a function of normalized chirp parameter F, and apodization α. The graph is normalized with respect to the theoretical transmission response of a device with zero chirp ($F = 0$), and zero apodization ($\alpha = 0$). A device with zero apodization implies a uniform intensity distribution of light across the waveguide grating. This can be achieved if the first star-coupler section consists of a multi-mode interference coupler [11]. However, in practice, use of an FPR before the arrayed-waveguide section causes the distribution of light across the waveguides to follow an approximately Gaussian distribution. Hence, although the graph indicates the general trend in reduction of device transmission with varying chirp and apodization, the calculation of excess insertion loss needs to be performed with respect to an AWG with the same degree of apodization but zero chirp.

We can use Fig. 9(b) to approximately calculate the expected extra insertion loss for the chirped device with characteristics depicted in Fig. 8(a). Assuming an AWG with apodization of $\alpha = 0.8$, and with zero chirp, Fig. 9(b) indicates an insertion loss of 1.76 dB relative to a device with no apodization and no chirping. The insertion loss associated with a device with apodization $\alpha = 0.8$ and chirp parameter $F = 11.2$ is 4.34 dB. Hence, the excess insertion loss due to the presence of chirp for this particular device is expected to be close to 2.58 dB. For a chirped AWG with maximum dispersion at the center of the passband given by $F = 17.6$ (see Fig. 7), Fig. 9(b) indicates the insertion loss to be 7.39 dB. Hence, we would expect the excess insertion loss through such a chirped AWG to be approximately 5.63 dB.

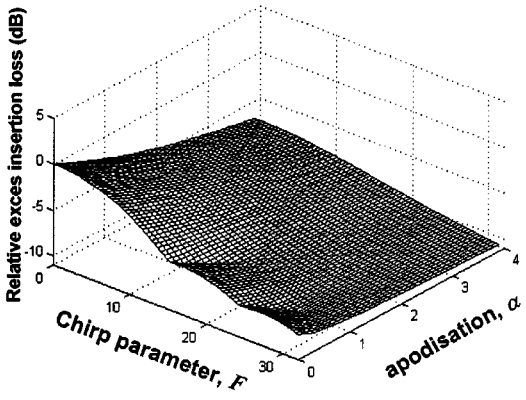

(a)

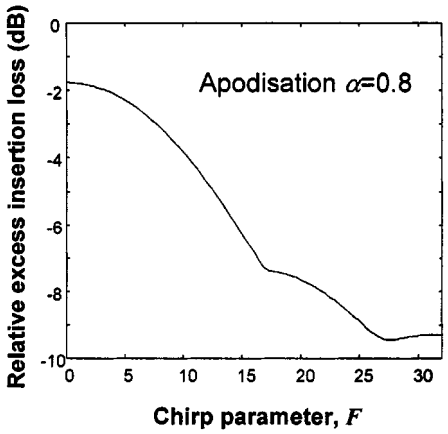

(b)

Fig. 9. (a) Variation of relative excess insertion loss as a function of AWG apodization α, and chirp parameter F. (b) Graph of variation of relative excess insertion loss as a function of chirp parameter F for an AWG with apodization $\alpha = 0.8$.

V. Conclusion

In conclusion, we have described how active AWGs may find a wide variety of application in future WDM networks. Simulations have shown that a novel holographic technique using individual phase-modulators in the waveguide-array allows amplifier gain equalization of 12 dB for 8×100 GHz spaced WDM channels, with interchannel ASE suppressed by greater than 20 dB. Optical add/drop multiplexing of arbitrary channels has also been simulated with channel suppression of 15 dB. The filter channel response has also been broadened to near-rectangular, providing greater tolerance to temperature effects and wavelength fluctuations. These holographic designs are robust to individual phase-modulator failures and fabrication phase errors. We have also described further WDM functionality achieved through dispersion compensation of up to ± 300 ps/nm using a hybrid Fourier–Fresnel AWG. In principle, further higher order polynomial-profiled active regions could be added to the AWG Fourier plane, to achieve dynamic compensation for the higher order dispersion effects which are becoming evident in high-capacity lightwave communication

systems. The associated tunable time-delay functionality may also alleviate time synchronization problems in emerging meshed-topology IP-routed networks.

REFERENCES

[1] A. Jourdan, F. Masetti, M. Garnot, G. Soulage, and M. Sotom, "Design and implementation of a fully reconfigurable all-optical crossconnect for high capacity multiwavelength transport networks," *J. Lightwave Technol.*, vol. 14, pp. 1198–1206, June 1996.

[2] A. E. Willner, "Systems issues for WDM components," in *IEEE-LEOS Summer Topical Meeting on WDM Components Technology*, Aug. 1997, pp. 5–6.

[3] M. K. Smit, "New focusing and dispersive planar component based on an optical phased array," *Electron. Lett.*, vol. 24, pp. 385–386, 1988.

[4] C. Dragone, C. A. Edwards, and R. C. Kistler, "An $N \times N$ optical multiplexer using a planar arrangement of two star couplers," *IEEE Photon. Technol. Lett.*, vol. 3, pp. 812–815, Sept. 1991.

[5] G. R. Hill, "A wavelength routeing approach to optical communication networks," *Br. Telecom. Technol. J.*, vol. 6, pp. 24–31, 1988.

[6] M. C. Parker, F. Farjady, and S. D. Walker, "Wavelength-tolerant optical access architectures featuring N-dimensional addressing and cascaded arrayed-waveguide gratings," *J. Lightwave Technol., Special Issue on Photonic Switching Systems, Technologies, and Techniques*, vol. 16, no. 12, pp. 2296–2302, 1998.

[7] ——, "Application of synthetic aperture techniques to arrayed-waveguide grating passband control," in *Proc. IPR'98*, Victoria, B.C., Canada, Mar. 1998.

[8] M. C. Parker and S. D. Walker, "Design of arrayed-waveguide gratings using hybrid Fourier–Fresnel transform techniques," *IEEE J. Special Topics in Quantum Electronics on Fiber-Optic Passive Components*, vol. 5, no. 5, pp. 1379–1384, 1999.

[9] M. C. Parker, A. D. Cohen, and R. J. Mears, "Dynamic digital holographic wavelength filtering," *J. Lightwave Technol.*, vol. 16, no. 7, pp. 1259–1270, 1998.

[10] C. Madsen and J. Zhao, *Optical Filter Design and Analysis: A Signal Processing Approach*. New York: Wiley, 1999.

[11] M. R. Amersfoort, J. B. D. Soole, H. P. LeBlanc, N. C. Andreakis, A. Rajhel, and C. Caneau, "Passband broadening of integrated arrayed-waveguide filters using multimode interference couplers," *Electron. Lett.*, vol. 32, no. 5, pp. 449–451, 1996.

[12] C. Dragone, "Efficient techniques for widening the passband of a wavelength router," *J. Lightwave Technol.*, vol. 16, no. 10, pp. 1895–1906, 1998.

[13] M. Born and E. Wolf, *Principles of Optics*, 6th ed. New York: Pergamon, pp. 382–386.

[14] M. C. Parker, A. D. Cohen, and R. J. Mears, "Dynamic holographic spectral equalization for WDM," *IEEE Photon. Technol. Lett.*, vol. 9, pp. 529–531, Apr. 1997.

[15] A. D. Cohen, M. C. Parker, and R. J. Mears, "Active management of 100-GHz-spaced WDM channels," in *Proc. OFC'99*, San Diego, CA, Feb. 1999.

[16] D. H. P. Maat, F. H. Groen, R. C. Horsten, Y. C. Zhu, P. E. W. Kruis, C. G. P. Herben, X. J. M. Leijtens, and M. K. Smit, "Tunable phase array demultiplexer on InP featuring wide-range tuning and passband shaping," in *Proc. ECIO'99*, Turin, Italy, Apr. 1999, Post-Deadline Paper.

[17] S. M. Jackson, P. D. Hewitt, G. T. Reed, C. K. Tang, A. G. R. Evans, J. Clark, C. Aveyard, and F. Namavar, "A novel optical phase modulator design suitable for phased arrays," *J. Lightwave Technol.*, vol. 16, no. 11, pp. 2016–2019, 1998.

[18] M. A. Seldowitz, J. P. Allebach, and D. W. Sweeney, "Synthesis of holograms by direct binary search," *Appl. Opt.*, vol. 26, no. 14, pp. 2788–2798, 1987.

[19] S. Weissbach, F. Wyrowski, and O. Bryngdahl, "Digital phase holograms: Coding and quantization with an error diffusion concept," *Opt. Commun.*, vol. 72, no. 1, pp. 37–41, 1989.

[20] C. R. Doerr, M. Cappuzzo, E. Laskowski, A. Paunescu, L. Gomez, L. W. Stulz, and J. Gates, "Dynamic wavelength equalizer in silica using the single-filtered-arm interferometer," *IEEE Photon. Technol. Lett.*, vol. 11, pp. 581–583, May 1999.

[21] A. Yiptong, M. C. Parker, and R. J. Mears, "Active arrayed-waveguide gratings for equalization and WDM channel management," in *Proc. IPR'99*, Santa Barbara, CA, July 1999, Paper RTuJ4.

[22] A. D. Cohen, M. C. Parker, and R. J. Mears, "100-GHz-resolution dynamic holographic channel management for WDM," *IEEE Photon. Technol. Lett.*, vol. 11, pp. 851–853, July 1999.

[23] F. Ouellette, J.-F. Cliché, and S. Gagnon, "All-fiber devices for chromatic dispersion compensation based on chirped distributed resonant coupling," *J. Lightwave Technol.*, vol. 12, pp. 1727–1738, 1994.

[24] B. J. Eggleton, J. A. Rogers, P. S. Westbrook, and T. A. Strasser, "Electrically tunable power efficient dispersion compensating fiber Bragg grating," *IEEE Photon. Technol. Lett.*, vol. 11, pp. 854–856, July 1999.

[25] G. Lenz, B. J. Eggleton, C. K. Madsen, C. R. Giles, and G. Nykolak, "Optimal dispersion of optical filters for WDM systems," *IEEE Photon. Technol. Lett.*, vol. 10, pp. 567–569, Apr. 1998.

[26] A. J. Lowery and P. C. R. Gurney, "270-km 10Gbit/s WDM dispersion compensation using a chirped AWGM," in *Proc. OFC'99*, San Diego, CA, Feb. 1999, Paper FD5.

[27] M. Abramowitz and I. A. Stegun, *Handbook of Mathematical Functions*, 9th ed. New York: Dover, sec. 7.3.3.1 & 7.3.4.1, p. 300.

[28] H. Kogelnik, "Filter response of nonuniform almost-periodic structures," *Bell Syst. Tech. J.*, vol. 55, no. 1, pp. 109–126, 1976.

[29] M. Born and E. Wolf, *Principles of Optics*, 6th ed. New York: Pergamon, pp. 428–433.

[30] M. C. Parker and S. D. Walker, "Dynamic dispersion compensation using a parabolic phase apertured active arrayed-waveguide grating," in *Proc. IPR'99*, Santa Barbara, CA, July 1999, Paper RTuJ3.

Michael C. Parker (A'96) was born in London, England, in 1971. He graduated with a first class B.A. degree in electrical and information sciences from Cambridge University, U.K., in 1992.

He spent six-months working for Carl Zeiss, Germany, developing large-field objectives for use in photolithographic steppers, before commencing his Ph.D. degree in optical communications at Cambridge University. There he conducted research into holographic space/wavelength (WDM) switches using free-space ferroelectric liquid crystal spatial light modulators, and completed his Ph.D. in 1996. Since 1997, he has been working for Fujitsu Telecommunications Europe Ltd., based in Colchester, U.K., conducting research into WDM optical access networks and associated technologies, such as AWG design and theory, dispersion compensation techniques, dynamic optical add/drop multiplexers and novel distributed grating structures. Since 2000, he has also been appointed a Principal Researcher of the Photonics Networking Laboratory, Fujitsu Network Communications, Richardson, Texas; and has also been accorded the title Visiting Fujitsu Senior Research Fellow by the University of Essex, U.K. He has filed seven patents and has authored over 50 publications.

Dr. Parker is an associate member of the IEE and a member of the Optical Society of America (OSA).

Stuart D. Walker was born in Dover, England, in 1952. He received the B.Sc. degree in physics from Manchester University, U.K., in 1973 and the M.Sc. and Ph.D. degrees from the University of Essex, U.K., in 1975 and 1981, respectively.

After completing a period of contractual work for British Telecom Laboratories between 1979 and 1982, he joined as a staff member in 1982. He worked on various aspects of optical system design and was promoted to Head of the Regenerator Design Group in 1987. Since 1988, he has been Senior Lecturer in Optical Communication at the University of Essex. His current research interests are concerned with the modeling and analysis of advanced optical network components and systems.

Augustin Yiptong, photograph and biography not available at the time of publication.

Robert J. Mears, photograph and biography not available at the time of publication.